Liquid Crystalline and Monotropic Phase Behaviors of 2,3,6,7,10,11-Hexa(4′-octyloxybenzoyloxy)triphenylene Discotic Molecules

Benjamin Y. Tang, Jason J. Ge, Anqiu Zhang, Bret Calhoun, Peihwei Chu, Huabin Wang, Zhihao Shen, Frank W. Harris, and Stephen Z. D. Cheng*

Maurice Morton Institute and Department of Polymer Science, The University of Akron, Akron, Ohio 44325-3909

Received August 25, 2000. Revised Manuscript Received October 30, 2000

Multiple phase transitions and monotropic phase behavior are observed in a discotic liquid crystal, 2,3,6,7,10,11-hexa(4′-octyloxybenzoyloxy)triphenylene (HOBT-C8). Detailed phase structural analyses using wide-angle X-ray diffraction and electron diffraction show that, in addition to a discotic nematic (N_D) phase at high temperatures, a rectangular columnar (Φ_R) phase and an orthorhombic crystalline (K_I) phase developing sequentially upon cooling can be identified. A crystalline (K_{II}) phase with a higher melting temperature than that of the K_I phase forms during heating. Therefore, the K_I phase represents a metastable phase with respect to the K_{II} phase, and the more stable K_{II} phase can be bypassed during cooling at relatively fast cooling rates. The K_I phase is thus monotropic with respect to the K_{II} phase at relatively slow heating rates. The optical texture of each phase can be distinguished from polarized light microscopy. A relationship between Gibbs free energy and temperature for different phases can be constructed, which thermodynamically and kinetically represents these multiple phase transitions and the monotropic phase behavior of the K_I phase.

Introduction

Ever since the discovery of discotic liquid crystals (LCs) and their columnar phases in 1977,[1] a large amount of attention has been paid to this class of LC materials because of their tremendous application potentials in photonic and electronic areas. Disklike molecules intrinsically possess a flat, rigid, and rotationally symmetric core connected with flexible tails. The core structures are commonly constructed by a single phenylene group,[1,2] several phenylene groups,[2−6] metal ion complexes,[7−11] or self-assembled disk-shaped systems.[12−14] The flexible tails, which are alkyl chains in most cases, sometimes bearing functional end groups,[15] are necessary to form discotic LC phases.

Most disklike molecules show nematic (N_D) and columnar (Φ) phases.[1,3,4] Unlike rodlike LCs, which have their molecular orientation director parallel to the molecular long axis, the director of disklike molecules is defined to be perpendicular to the disk plane. The N_D phase is formed by randomly stacking disks one on the top of another along with a preferential director orientation. The lateral packing of disks in the N_D phase is of short-range order. Disklike molecules can also form higher ordered LC phases, which possess a characteristic feature of forming columns of these molecules by stacking disks in a more regular manner. Therefore, various lateral packings of these columnar (Φ) phases can be constructed such as rectangular (Φ_R), hexagonal (Φ_H), tilted (Φ_T), or oblique (Φ_{OB}) columnar phases.[2−4,16] These disklike molecules can be connected to each other to form main-chain LC polymers or to another backbone polymer to form side-chain LC polymers. Both side-chain[17,18] and main-chain[19,20] LC polymers containing discotic mesogens have a tendency to form columnar phases. Ordered discotic networks with stabilized Φ

* To whom correspondence should be addressed. E-mail: cheng@polymer.uakron.edu.

(1) Chandrasekhar, S.; Sadashiva, B. K.; Suresh, K. A. *Pramana* **1977**, *9*, 471.
(2) Chandrasekhar, S. *Mol. Cryst. Liq. Cryst.* **1981**, *63*, 171.
(3) Destrade, C.; Nguyen Huu Tinh; Gasparoux, H.; Malhtete, J.; Levelut, A. M. *Mol. Cryst. Liq. Cryst.* **1981**, *71*, 111.
(4) Nguyen Huu Tinh; Gasparoux, H.; Destrade, C. *Mol. Cryst. Liq. Cryst.* **1981**, *68*, 101.
(5) Billard, J.; Dubois, J. C.; Vaucher, C.; Levelut, A. M. *Mol. Cryst. Liq. Cryst.* **1981**, *66*, 115.
(6) Pugh, C.; Percec, V. *J. Mater. Chem.* **1991**, *1*, 765.
(7) Giroud-Godquin, A. M.; Billard, J. *Mol. Cryst. Liq. Cryst.* **1981**, *66*, 147.
(8) Piechocky, C.; Simon, J.; Skoulios, A.; Guillon, D.; Weber, P. *J. Am. Chem. Soc.* **1982**, *104*, 5245.
(9) Barbera, J.; Cativiela, C.; Serrano, J. L.; Zurbano. M. M. *Adv. Mater.* **1991**, *3*, 602.
(10) Zhang, H.; Lai, C. K.; Swager, T. *Chem. Mater.* **1995**, *7*, 2067.
(11) Lai, C. K.; Tsai, C.-H.; Pang, Y.-S. *J. Mater. Chem.* **1998**, *8*, 1355.
(12) Ebert, E.; Wendorff, J.; Lattermann, G. *Liq. Cryst.* **1990**, *7*, 553.
(13) Lattermann, G.; Straufer, G.; Brezesinski, G. *Liq. Cryst.* **1991**, *10*, 169.
(14) Ciuchi, F.; Nicola, G. D.; Franz, H.; Gottarelli, G.; Mariani, P.; Bossi, M. G. P.; Spada, G. P. *J. Am. Chem. Soc.* **1994**, *116*, 7064.
(15) Farre-Nicolin, C. D.; Lub, J.; Van der Sluis, P. *Adv. Mater.* **1996**, *8*, 1005.
(16) Destrade, C.; Foucher, P.; Gasparoux, H.; Nguyen Huu Tinh; Levelut, A. M.; Malthete, J. *Mol. Cryst. Liq. Cryst.* **1984**, *106*, 121.
(17) Kreuder, W.; Ringsdorf, H. *Macromol. Chem. Rapid Commun.* **1983**, *4*, 807.
(18) Weck, M.; Mohr, B.; Maughon, B. R.; Grubbs, R. H. *Macromolecules* **1997**, *30*, 6430.
(19) Raja, K. S.; Raghanathan, V. A.; Ramakrishnan, S. *Macromolecules* **1998**, *31*, 3807.
(20) Wang, T.; Yan, D.; Zhou, E.; Karthaus, O.; Ringsdorf, H. *Polymer* **1998**, *39*, 4509.

10.1021/cm0006897 CCC: $20.00
Published on Web 12/12/2000

mesophases using cross-linkable chain ends have also been reported.[21] Recent work has shown that some non-disk molecules can be self-assembled into Φ phases.[12−14] Columnar phase formation in numerous LC polymers with rodlike mesogens has also been reported.[22−25]

To precisely distinguish the structural symmetry and order of discotic LC phases, such as Φ_R, Φ_H, Φ_T, or Φ_{OB} columnar phases, more sophisticated approaches and careful measurements are necessary, since, generally speaking, these structures only possess two-dimensional order. In the disk-stacking direction, only a short-range order exists.[26] A few reports of structural determination on the discotic crystalline and LC phases can be found.[27] Most discotic LCs show polymorphism,[2,4,16] that is multiple LC phase transitions. Crystal phase transitions can be observed by changing temperatures at a constant pressure. These transitions are normally reversible during the cooling/heating process. Some truxene derivatives exhibit an unusual inverted nematic−columnar transition sequence;[28] that is, the less-ordered nematic phase occurs at a lower temperature while the higher ordered columnar phase can be found at a higher temperature.

Monotropic phase behavior in small molecules and polymers has been observed.[29−37] Both monotropic and enantiotropic behaviors in columnar hexagonal phases of a series of metallomesogenic discotic LCs have also been reported.[11] The monotropic phase exists only when the more stable phase is bypassed due to the fact that the necessity of undercooling is required to overcome the free energy barrier for forming this stable phase during cooling.

In this publication, phase transition behaviors of a discotic LC compound, 2,3,6,7,10,11-hexa(4′-octyloxybenzoyloxy)triphenylene, HOBT-C8, are reported. It is observed that this discotic LC exhibits complicated phase transition behaviors including monotropic phase behavior. In the literature, detailed phase behaviors of HOBT-C*n* (*n* = even numbers) discotic compounds have not been reported. This motivated our research interests in this series of materials, of which the discotic LC HOBT-C8 investigated here serves as an example. These compounds can also be modified to have potential applications in developing compensation layers with a tilted optical axis in liquid crystal displays.[38]

Experimental Section

Material and Sample Preparations. The discotic LC compound HOBT-C8 was synthesized and purified following the procedure described in ref 4. The chemical structure is shown below:

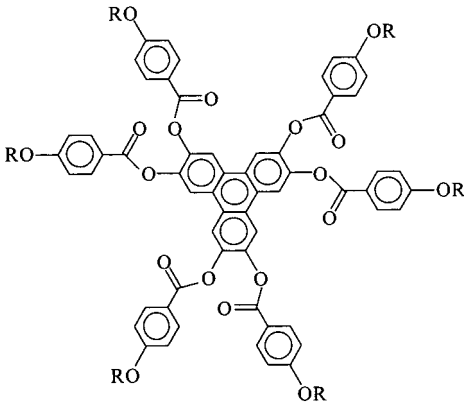

The sample was vacuum-dried before carrying out any characterization and analysis. For differential scanning calorimetry (DSC) experiments, the sample weight was about 2.5 mg and the pan weights were kept constant with a precision of ±0.001 mg. To determine different phase structures, samples having a thickness of around 0.5 mm for both wide-angle X-ray diffraction (WAXD) powder (one-dimensional, 1D) and oriented (two-dimensional, 2D) experiments were prepared. The oriented samples were obtained via mechanical shearing. To prepare TEM and ED thin film samples, a dilute solution of HOBT-C8 in xylene (0.5 wt %) was used to cast thin films onto carbon-coated glass substrates, followed by solvent evaporation and thermal treatments. The thickness ranged between 50 and 100 nm.

The isotropization of HOBT-C8 occurred at a high temperature of 239 °C with a heat of transition of $N_D \rightarrow$ isotropic melt (I) of 0.5 kJ/mol measured by DSC. To avoid sample decomposition and oxidation, while still eliminating the previous thermal history, the samples for DSC and WAXD experiments performed in this study were only heated to 180 °C in the N_D phase (above the $\Phi_R \rightarrow N_D$ transition temperature of 171 °C) instead of the isotropic melt. The sample fluidity was high, and the sample was almost transparent in the N_D phase.

Equipment and Experiments. A Perkin-Elmer DSC-7 with a cooling refrigerator was used for DSC experiments. The calibration of temperature and heat of transition was performed using standard materials (benzoic acid and indium) at different scanning rates. The onset temperatures instead of the peak temperatures were used to describe the transition temperatures. For cooling scans, the onset temperatures were obtained on the high-temperature side, while the low-temperature side onsets were used for heating scans.

The WAXD equipment consists of a Rigaku 18 kW rotating anode (Cu Kα) X-ray generator and an erasable image plate with 1500 pixels × 1500 pixels. A graphite crystal was inserted into the beam as the monochromator. The X-ray beam was circularly focused with a tubular collimator (0.3 mm in

(21) Disch, S.; Finkelmann, H.; Ringsdorf, H.; Schuhmacher, P. *Macromolecules* **1995**, *28* (8), 2424.
(22) Ungar, G. *Polymer* **1993**, *34*, 2050.
(23) Zheng, R.; Chen, R.; Cheng, S. Z. D.; Xie, F.; Yan, D.; He, T.; Percec, V.; Chu, P.; Ungar, G. *Macromolecules* **1999**, *32*, 3574.
(24) Zheng, R.; Chen, R.; Cheng, S. Z. D.; Xie, F.; Yan, D.; He, T.; Percec, V.; Chu, P.; Ungar, G. *Macromolecules* **1999**, *32*, 6981.
(25) Zheng, R.; Chen, R.; Cheng, S. Z. D.; Xie, F.; Yan, D.; He, T.; Percec, V.; Chu, P.; Ungar, G. *Macromolecules* **2000**, *33*, 5159.
(26) De Gennes, P. G.; Prost, J. *The Physics of Liquid Crystals*, 2nd ed.; Clarendon Press: Oxford, 1993.
(27) Voigt-Martin, I. G.; Grabella, R. W.; Schumacher, M. *Liq. Cryst.* **1994**, *17*, 775.
(28) Destrade, C.; Gasparoux, H.; Barbera, J.; Nguyen Huu Tinh; Malthete, J. *Mol. Cryst. Liq. Cryst.* **1981**, *67*, 37.
(29) Carr, N.; Gray, G. W. *Mol. Cryst. Liq. Cryst.* **1985**, *124*, 27.
(30) Andrews, B. M.; Gray, G. W. *Mol. Cryst. Liq. Cryst.* **1985**, *123*, 257.
(31) Ungar, G.; Feijoo, J. L.; Keller, A.; Yord, R.; Percec, V. *Macromolecules* **1990**, *23*, 3411.
(32) Percec, V.; Keller, A. *Macromolecules* **1990**, *23*, 4347.
(33) Cheng, S. Z. D.; Yandrasits, M. A.; Percec, V. *Polymer* **1991**, *32*, 1284.
(34) Yandrasits, M. A.; Cheng, S. Z. D.; Zhang, A.; Cheng, J.; Wunderlich, B.; Percec, V. *Macromolecules* **1992**, *25*, 2112.
(35) Pardy, R.; Zhang, A.; Gabori, P. A.; Harris, F. W.; Cheng, S. Z. D.; Aducci, J.; Facinelli, J. V.; Lenz, R. W. *Macromolecules* **1992**, *25*, 5060.
(36) Pardey, R.; Shen, D.; Gabori, P. A.; Harris, F. W.; Cheng, S. Z. D.; Aducci, J.; Facinelli, J. V.; Lenz, R. W. *Macromolecules* **1993**, *26*, 3687.
(37) Ge, J. J.; Zhang, A.; McCreight, K. W.; Ho, R.-M.; Wang, S.-Y.; Jin, X.; Harris, F. W.; Cheng, S. Z. D. *Macromolecules* **1997**, *30*, 6498.
(38) Mori, H.; Itoh, Y.; Nishiura, Y.; Nakamura, T.; Shinagawa, Y. *Jpn. J. Appl. Phys.* **1997**, *36*, 143.

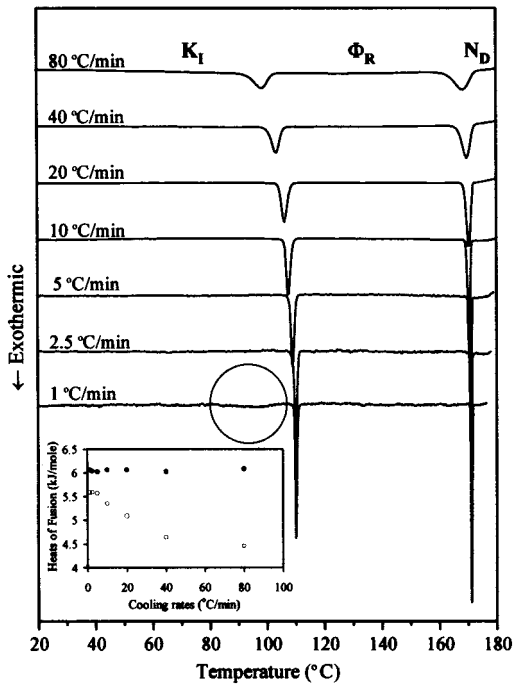

Figure 1. DSC cooling curves of HOBT-C8 at different rates. The inset shows the heats of transitions from $N_D \rightarrow \Phi_R$ (closed circle) and $\Phi_R \rightarrow K_I$ (open circle) as a function of cooling rates.

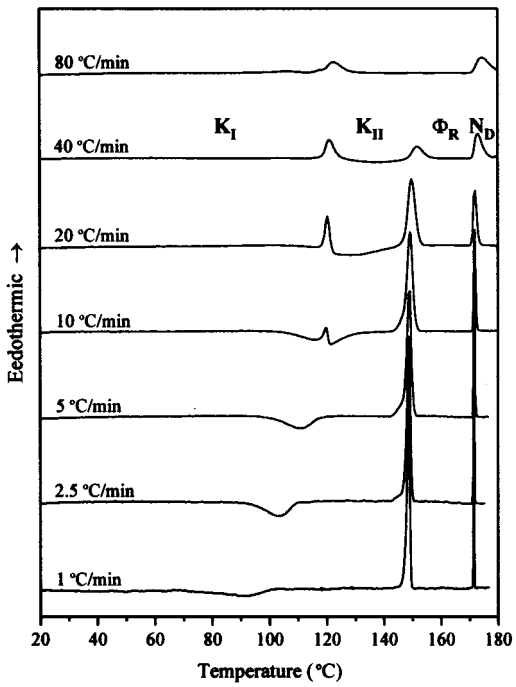

Figure 2. DSC heating curves of HOBT-C8 at different rates.

diameter). The distance between sample and image plate was set to be 200 mm. The diffraction angle was calibrated using silicon powder crystals for the high-angle region ($2\theta > 15°$) and silver behenate crystals for the low-angle region ($2\theta < 15°$). The exposure time was varied between 10 and 200 min, depending on the sample diffraction intensity. 1D powder patterns were obtained through an angular integration of the 2D images. Various thermal treatments were specifically used during the WAXD measurements to determine crystal structures using the reciprocal lattice approach and refinement, as commonly established in X-ray fiber diffraction.[39]

An Olympus (HB-2) polarized light microscope (PLM) coupled with a Mettler (FP90) hot stage was utilized for optical texture observations. The sample sandwiched between a glass slide and a cover glass was about 10 μm thick. A JEOL (1200 EX II) TEM with a 120 kV acceleration voltage was used to study morphology and structure. The thermal histories of the thin films were kept the same as those of the DSC and WAXD samples. The thin films were shadowed by platinum. For electron diffraction (ED), the camera length was set to be 160 cm and the crystal lattice spacings were calibrated using TlCl crystals.

Results and Discussion

Phase Transitions Observed in DSC. Figure 1 shows a set of DSC cooling curves of HOBT-C8 at different rates. Two exothermic peaks (corresponding to transitions from the $N_D \rightarrow \Phi_R$ and $\Phi_R \rightarrow K_I$ phases; see the following section of structural determinations) are observed on all cooling scans. The onset temperature for the high-temperature transition is at 171 °C, being independent of the cooling rates. The low-temperature transition shows cooling-rate dependence with onset temperatures shifting from 102 °C at 80 °C/min to 112 °C at 1 °C/min. A third broad exothermic process, which is highlighted with a circle in Figure 1, represents another transition between 80 and 105 °C observed only at a cooling rate of 1 °C/min. With increasing cooling rate, this process vanishes.

A plot of heats of transitions for the high- and low-temperature transitions (ΔH) versus cooling rates is shown in an inset of Figure 1. It is evident that the ΔH of 6.1 kJ/mol of the high-temperature transition is independent of cooling rates. However, the ΔH of the low-temperature transition increases with the decreasing of cooling rates. The maximum value of ΔH of the low-temperature transition reaches a constant of 5.6 kJ/mol when the cooling rate is slower than 5 °C/min. The cooling-rate independence of both the transition temperature and the ΔH of the high-temperature transition implies that this transition is associated with the LC structural transformation (the $N_D \rightarrow \Phi_R$ transition; see below). On the other hand, the cooling-rate dependence of both parameters for the low-temperature transition (the $\Phi_R \rightarrow K_I$ transition; see below) suggests that this transition involves a crystalline phase transformation.

The subsequent DSC heating curves are presented in Figure 2. Two endothermic processes corresponding to those observed during cooling are evident when the sample is heated at a rate of 80 °C/min. Another new endothermic peak at 148 °C appears accompanied by an exothermic process between ~125 and ~140 °C at a heating rate of 40 °C/min. With further decreasing the heating rates (between 40 and 10 °C/min), this exothermic process becomes partially overlapped with the low-temperature endothermic peak. It takes place at much lower temperatures than the low-temperature transition at 118 °C when the heating rates further decrease. Therefore, when the cooling rate is less than or equal to 5 °C/min, the endothermic low-temperature transition cannot be observed. This indicates that, before reaching the melting temperature of this phase, it completely transfers to a phase having a higher melting temperature of 148 °C. A relatively large heat of transition (up to 19.9 kJ/mol) can also be found. Furthermore, it

(39) Eshoo, M.; Wu, Z.; Anqiu Zhang, A.; Shen, D.; Tse, C.; Harris, F. W.; Cheng, S. Z. D.; Gardner, K. H.; Hsiao, NB. S. *Macromol. Chem. Phys.* **1994**, *195*, 2207.

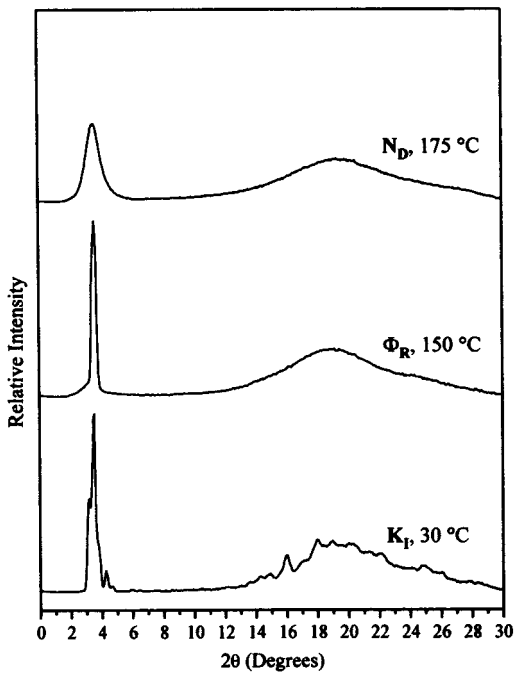

Figure 3. WAXD powder pattern of HOBT-C8 during cooling at 5 °C/min.

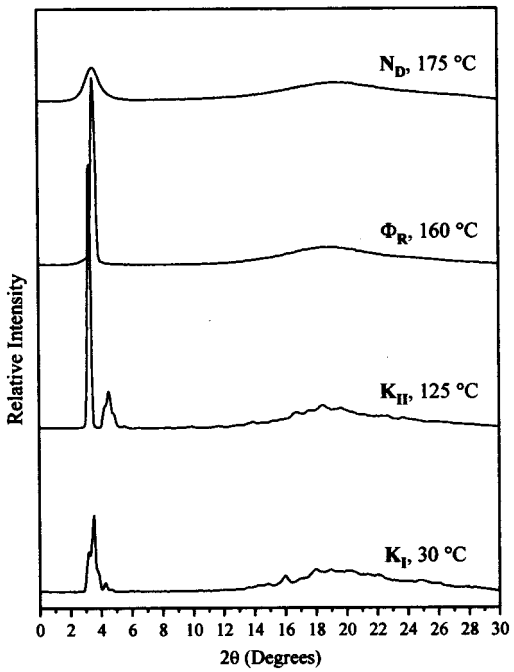

Figure 4. WAXD powder pattern of HOBT-C8 during heating at 5 °C/min.

appears that these two phases are competitive; namely, the new phase formation is at the expense of the low-temperature phase.

Phase Identifications Using WAXD Powder Patterns. 1D WAXD powder patterns (transmission mode) during cooling at 5 °C/min are shown in Figure 3. Two amorphous halos can be seen at 175 °C. One at a high angle of $2\theta = 19.5°$ ($d = 0.45$ nm) represents the average intermolecular distance, and another at a low angle of $2\theta = 3.7°$ (d spacing of 2.39 nm) is attributed to the average distance between disks. This is a characteristic feature of discotic LCs in a N_D phase. Passing through the transition at 171 °C, the WAXD result measured at 150 °C in Figure 3 exhibits significant differences in the low-angle region, which illustrates the formation of a new phase. Two overlapped sharp diffractions in this 2θ region can be identified, implied by the asymmetric peak shape (see the sheared 2D WAXD patterns below for more evidence). The high-angle amorphous halo does not change its shape except a slight shift of the peak maximum from 19.5° to 18.9° during this phase transition. This phase is most likely a LC phase which possesses supramolecular order in the discotic molecular packing (assigned as a Φ_R phase; see below for detailed analysis). According to the DSC results in Figure 1, HOBT-C8 reaches another phase below 110 °C. As shown in Figure 3 at 30 °C, several partially overlapped diffractions with 2θ maxima at 3.2°, 3.4°, 3.8°, 4.3°, and 4.7°, respectively, appear in the low-angle region. On the other hand, various relatively weak diffractions can also be observed in the high-angle region, indicating an introduction of crystalline orders in the discotic molecules. This low-temperature phase is assigned as the K_I phase (see below for detailed analysis).

Figure 4 illustrates the WAXD powder patterns of HOBT-C8 during heating at 5 °C/min. The DSC results in Figure 2 show that, after a crystallization exotherm between 94 and 123 °C, the K_I phase formed during cooling has transferred to another crystalline phase. This phase structure is represented by the WAXD powder pattern shown in Figure 4 at 125 °C. In the low-angle region of this pattern (Figure 4), a sharp diffraction at $2\theta = 3.3°$ can be clearly identified. Another three partially overlapped diffractions with 2θ maxima at 4.2°, 4.3°, and 4.5° and one relatively low intensity diffraction at $2\theta = 5.6°$ are evident. The intensities and positions for the high-angle diffractions also change after this phase transformation during heating. Several low-intensity diffractions appear in the 2θ region of 6−14°, which are not found in the WAXD powder pattern in the K_I phase obtained at 30 °C in Figure 4. Therefore, it is concluded that the new crystalline phase is formed and assigned as a K_{II} phase. At 160 °C, the K_{II} phase is already molten and the WAXD pattern basically returns to that shown in Figure 3 obtained at 150 °C during cooling (except for an enhanced intensity during heating). Again, this phase is assigned to be the Φ_R phase. By heating the sample to 175 °C, the Φ_R phase melts and a WAXD powder pattern of the N_D phase appears again, which possesses those two amorphous halos.

Rectangular Columnar Phase (Φ_R). To determine the structure of these ordered phases, 2D WAXD and ED experiments on sheared samples have been performed to obtain dimensionality information. For the Φ_R phase, the sample is sheared at 150 °C, followed by cooling to 130 °C to obtain the WAXD fiber pattern at this temperature. Figure 5a shows the sheared pattern of the Φ_R phase. The shearing direction is indicated with an arrow in this figure. On the equator, partially overlapped (110) and (200) diffraction arcs are observed, which are more obvious by performing angular integration as shown in Figure 5b. The peak positions of the (110) and (200) arcs are at $2\theta = 3.55°$ and 3.68°, respectively, corresponding to d spacing values of 2.49 and 2.40 nm.

Morphological and diffraction results observed in TEM and ED are shown in Figure 6. Room temperature WAXD experiments show that thin film samples quickly

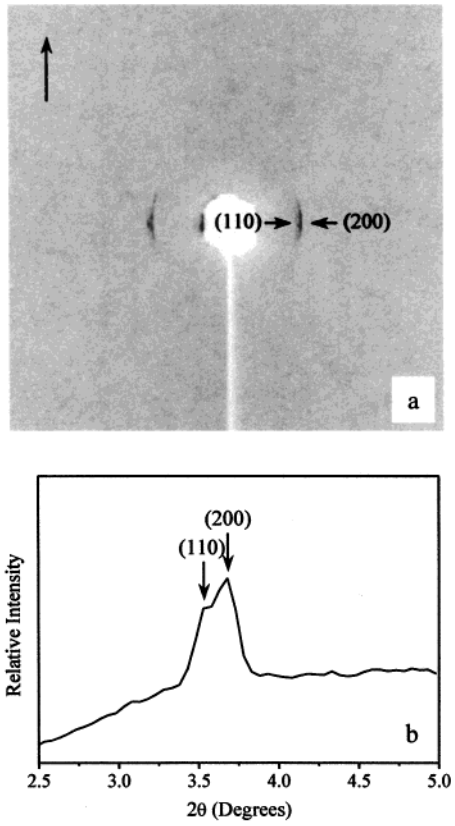

Figure 5. (a) Sheared 2D WAXD pattern of the Φ_R phase at 130 °C, and (b) angular integration of part a.

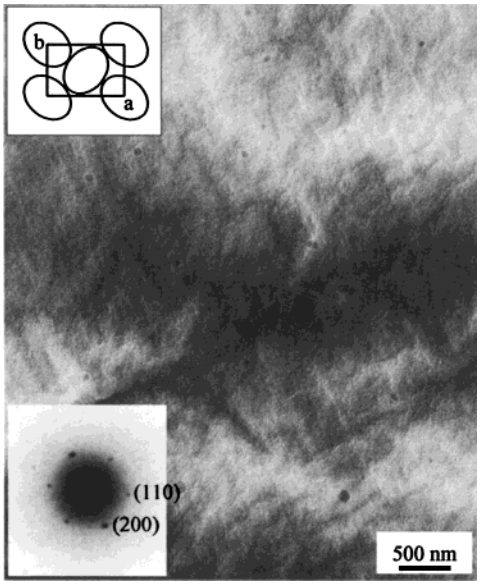

Figure 6. Morphology of the "frozen" Φ_R phase at room temperature (lower inset, the corresponding ED pattern; upper inset, a schematic 2D packing).

quenched into an ice water mixture from 150 °C possess the same Φ_R phase which was frozen by quenching. Figure 6 shows the morphology of the Φ_R phase, and one of the insets is the corresponding ED pattern. From this ED pattern, a preferential orientation along the [00*l*] zone diffraction can be found, indicating that the disks are in a flat-on arrangement. A stronger (200) diffraction matches the sheared WAXD results. The calculated *d* spacings for the (110) and (200) spots are

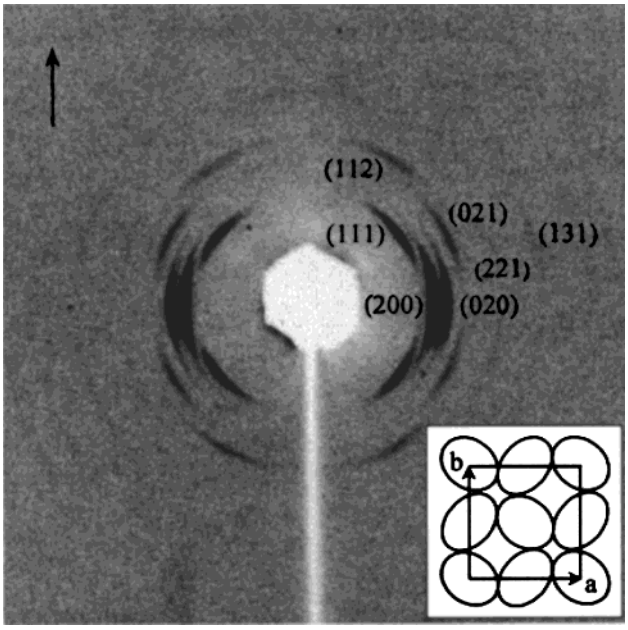

Figure 7. Sheared 2D WAXD pattern of the K_I phase at room temperature (inset: a schematic 2D packing).

Table 1. Indices, Measured and Calculated 2θ Angles, and *d* Spacing of the Orthorhombic K_I Phase

	2θ (deg)		*d* spacing (nm)	
indices	meas	calc	meas	calc
(200)	3.45	3.44	2.558	2.565
(020)	3.80	3.79	2.322	2.329
(111)	3.20	3.21	2.758	2.749
(021)	4.28	4.26	2.062	2.072
(221)	5.39	5.47	1.638	1.614
(131)	6.40	6.25	1.379	1.412
(112)	4.69	4.65	1.882	1.898

2.49 and 2.40 nm, respectively, which leads to a rectangular columnar (Φ_R) phase with the 2D dimensions a = 4.80 nm and b = 2.91 nm. A schematic representation of the 2D packing is also shown in the other inset of Figure 6.

Orthorhombic Crystalline Phase (K_I). In the DSC results in Figures 1 and 2, the K_I phase forms during cooling. To identify this crystalline structure, an oriented sample was prepared by mechanical shearing at around 150 °C in the Φ_R phase and, then, gradually cooled to room temperature to obtain the K_I phase. The 2D WAXD pattern of the low-angle region is shown in Figure 7 (the arrow in the figure represents the shearing direction). There are two slightly overlapped strong diffraction arcs which can be assigned as the (200) and (020) arcs on the equator. There are five diffraction arcs in the quadrants. In the first layer of *hk*1, the (111) and (021) arcs are clear, while the (221) and (131) arcs are weak. The (112) arc is the only diffraction shown in the second layer of *hk*2. The crystalline structure can be determined to be orthorhombic on the basis of the reciprocal lattice approach. Table 1 lists the assigned indices, the measured and calculated 2θ angles, and the *d* spacing values. The calculated orthorhombic unit cell parameters are a = 5.14 nm, b = 4.66 nm, c = 4.55 nm, and $\alpha = \beta = \gamma = 90°$. A possible 2D packing is shown as the inset in Figure 7. Considering that each disk layer thickness is around 0.5 nm, nine disk molecules must be stacked together to construct one unit cell along the *c*-axis. The total number of disk molecules is 36 (4 × 9)

per unit cell. The density of this K_I phase is calculated to be 0.94 g/cm^3. Substantial effort has been made to obtain ED patterns of the K_I phase without success. Single crystals cannot be grown because the K_I phase is formed during relatively fast cooling and it is metastable in nature (also see below).

The Monoclinic Crystalline Phase (K_{II}). The K_{II} phase generally develops during heating of the sample and eventually becomes a stable phase. To obtain the oriented WAXD pattern of the K_{II} phase, samples were prepared by shearing in the Φ_R phase at 150 °C and then cooling to 115 °C and annealing at this temperature for 10 h. On the basis of the WAXD experiments, a single crystal-like structure with an area of 0.7 × 0.7 mm^2 can be found. This area was isolated and exposed to the X-ray beam through three orthogonal directions, as indicated with arrows in the insets of Figure 8.

The resulting 2D WAXD images are shown in Figure 8, and these WAXD patterns represent the three individual [010], [001], and [100] zones which were obtained by rotating the sample to align the X-ray beam shot from the front, side, and top directions, respectively. In Figure 8a, the [010] zone possesses a strong arc indexed as the (001) arc on the equator. The (200) diffraction on the meridian has a similar intensity as that of the (001) diffraction. In the quadrant, there are two weak diffraction arcs, the (101) and (201) arcs, in the first layer. It is evident that the *a**- and *c**-axes are perpendicular to each other. The [001] zone shown in Figure 8b exhibits an identical (200) arc as that of the [010] zone in Figure 8a. However, the (020) diffraction is now slightly off the equator. This can be proven by the fact that the 2θ angle of the (120) arc is larger than that of the ($\bar{1}$20) arc. It is thus concluded that the angle γ* between the *a**- and *b**-axes is 85.5°. To unambiguously identify this K_{II} phase structure, the [100] zone is needed, which illustrates the relationship between the *b**- and *c**-axes. The sample position is carefully adjusted to ensure that the *a*-axis is parallel to the incident beam. The resulting pattern of the [100] zone is shown in Figure 8c. Although the diffraction is weak due to the thickness effect of the sample (less than 0.1 mm), the (020) and (001) diffraction arcs in the equator and the meridian, respectively, can still be identified. Therefore, the *b**-axis is perpendicular to the *c**-axis.

The crystal lattice of this K_{II} phase is thus determined to be monoclinic. The indices, the measured and the calculated 2θ angles, and the *d* spacing values are listed in Table 2. The calculated unit cell parameters are a = 5.39 nm, b = 4.29 nm, c = 1.94 nm, $\alpha = \beta = 90°$, and γ = 94.5°. Compared to the case of the K_I phase, the *a*-axis is ~5% larger and the *b*-axis is ~10% smaller and the angle between the *a*- and *b*-axes is now 4.5° deviated from 90° (see the inset in Figure 8c for a schematic representation of the real space 2D packing). The *c*-axis, however, decreases from 4.54 to 1.94 nm, indicating a substantial change of the number of molecules stacking along the *c*-direction. Since each disk thickness is around 0.5 nm, it is reasonable to assume four disk molecules stacking together along one *c*-repeat unit. A simple calculation shows that each disk molecule has a thickness of about 0.485 nm in the K_{II} phase but 0.505 nm in the K_I phase, which implies a possible denser packing of the K_{II} phase. The density calculation leads

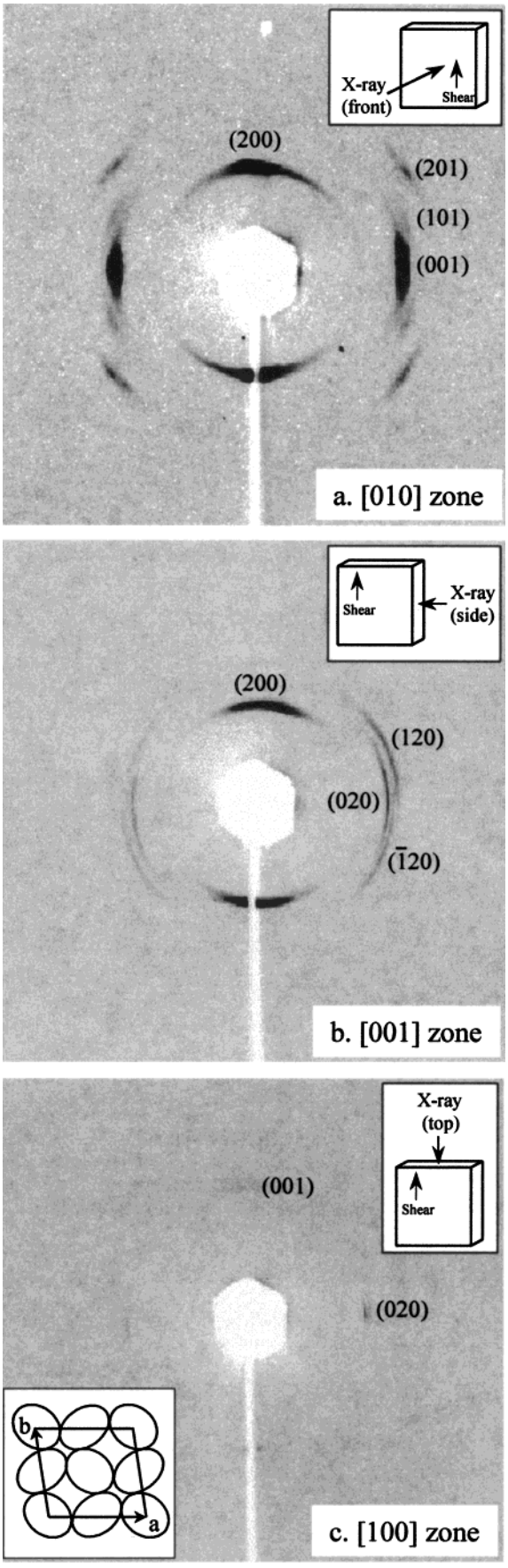

Figure 8. 2D WAXD patterns of a K_{II} single crystal-like domain at room temperature: (a) [010] zone; (b) [001] zone; and (c) [100] zone (upper insets, the corresponding X-ray beam directions; lower inset of part c, a schematic 2D packing).

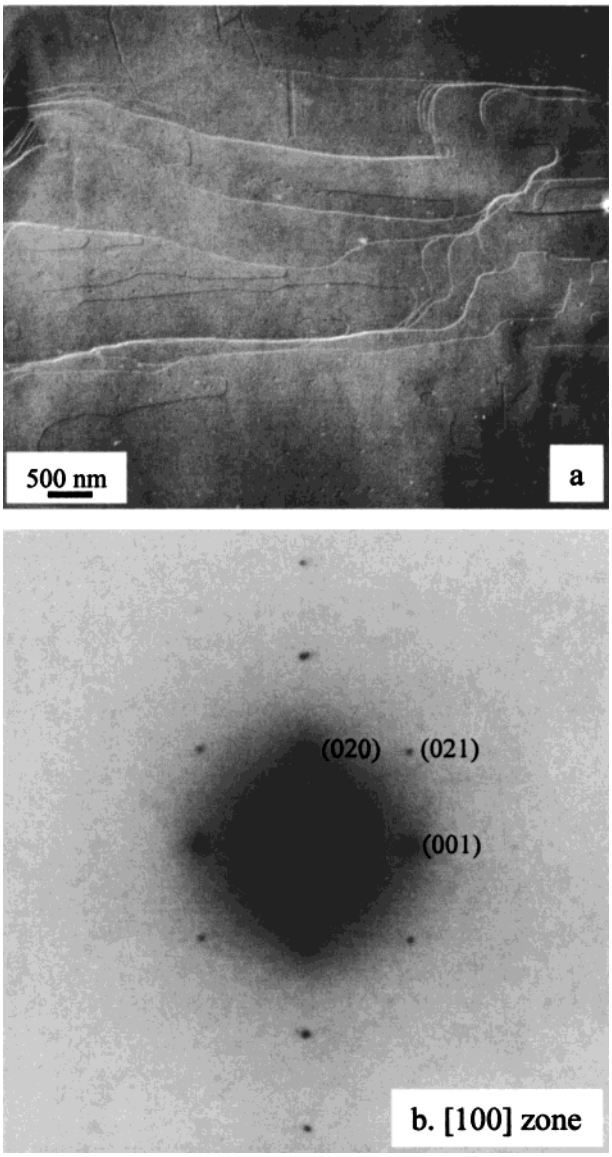

Figure 9. (a) TEM morphology of the K_{II} phase at room temperature, and (b) the corresponding ED pattern of part a, which is the [100] zone.

Table 2. Indices, Measured and Calculated 2θ Angles, and *d* Spacing of the Monoclinic K_{II} Phase

	2θ (deg)		*d* spacing (nm)	
indices	meas	calc	meas	calc
(200)	3.29	3.29	2.682	2.682
(020)	4.16	4.13	2.122	2.137
($1\bar{2}0$)	4.53	4.57	1.948	1.931
($\bar{1}20$)	4.31	4.32	2.048	2.043
(001)	4.53	4.55	1.948	1.940
(101)	4.88	4.84	1.809	1.824
(201)	5.61	5.62	1.573	1.571

to a value of 1.02 g/cm^3 ($4 \times 4 = 16$ molecules per unit cell).

To observe the TEM morphology and ED patterns of this K_{II} crystal, a thin film sample on carbon substrate was annealed at 115 °C for 10 h after cooling from 180 °C. The typical morphology and the corresponding ED pattern are shown in parts a and b, respectively, of Figure 9. The morphology is dominated by large flat-on stacking lamellar crystals. The ED pattern shown in Figure 10b is the [100] zone. The (001) and (020) diffractions are identical to those obtained in the sheared 2D WAXD pattern (Figure 8c), which further supports the WAXD observations and analyses.

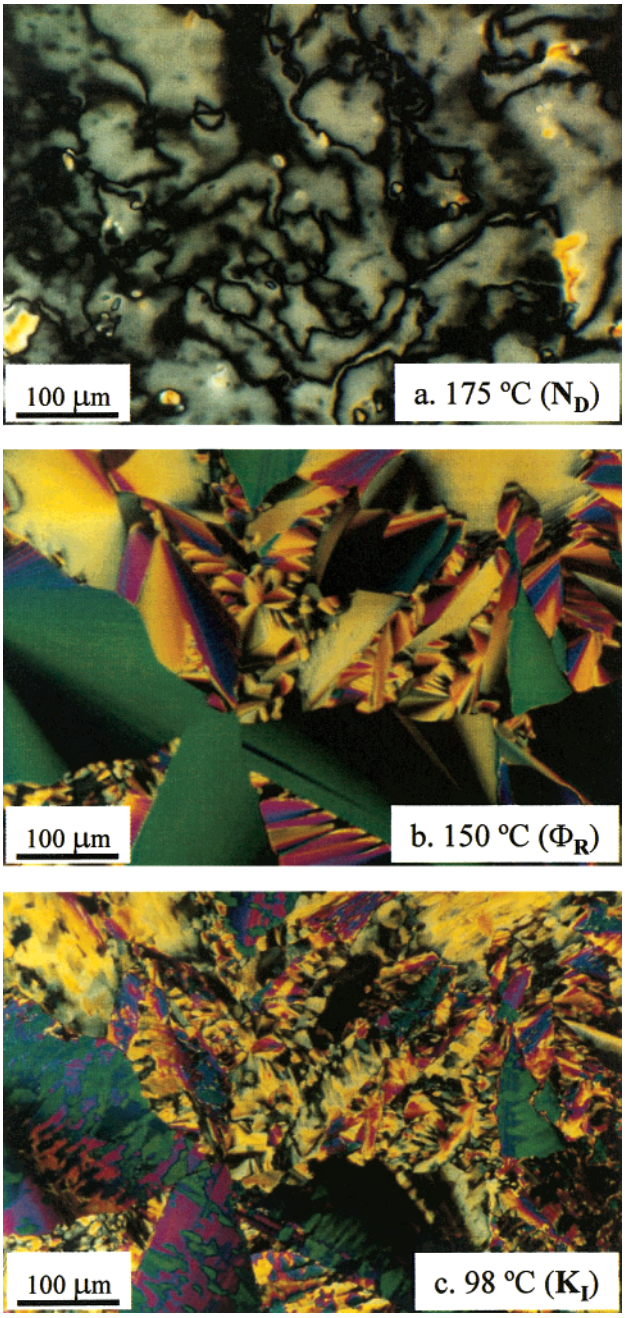

Figure 10. PLM photographs of HOBT-C8 during cooling at 5 °C/min: (a) a Schlieren texture of the N_D phase at 175 °C; (b) a fan-type focal conic texture of the Φ_R phase at 150 °C; and (c) a mosaic-like texture of the crystalline K_I phase at 98 °C.

Texture Observations in Different Phases. A series of PLM photographs at different temperatures, corresponding to different phases, have been taken during cooling (Figure 10) and heating (Figure 11) at 5 °C/min. Figure 10a shows a typical Schlieren texture at 175 °C, the characteristic texture of a nematic phase, which supports our assignment of the N_D phase. After the phase transition of $N_D \rightarrow \Phi_R$ at 171 °C, a fan-type focal conic texture can be seen at 150 °C (Figure 10b). Usually, this kind of texture can be observed for the hexagonal columnar phases, and here the texture belongs to the Φ_R phase on the basis of our WAXD and

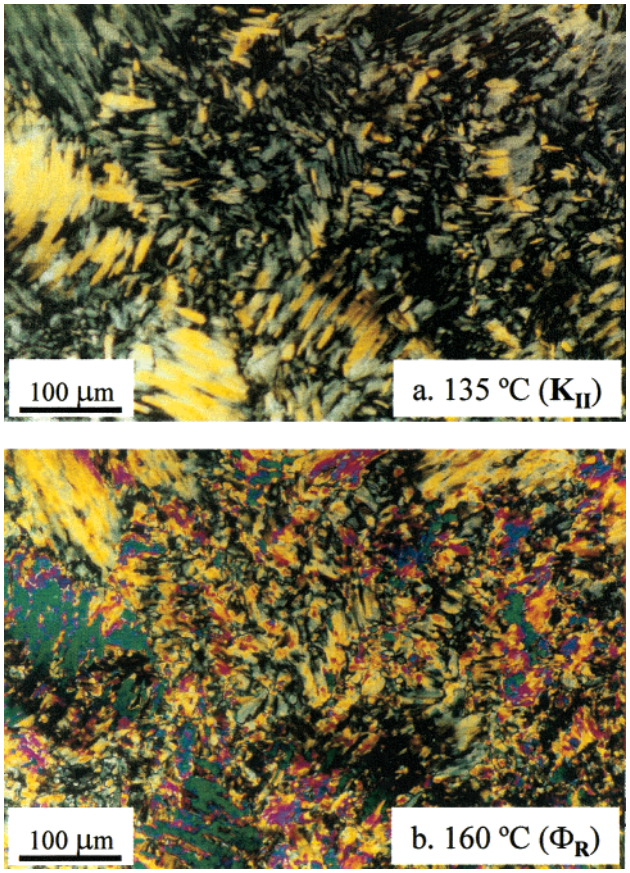

Figure 11. PLM photographs of HOBT-C8 during heating at 5 °C/min: (a) randomly oriented small crystals of the K_{II} phase at 135 °C; and (b) a small fan-type texture of the Φ_R phase at 160 °C.

ED results. Upon further cooling, a mosaic-like texture of the K_I phase is observed at 98 °C (Figure 10c). However, the major shape of the previous fan-type texture remains.

By heating at 5 °C/min to 135 °C, Figure 11a shows that the K_{II} phase in a PLM has fully developed and exhibits randomly oriented small crystals. After the melting of the K_{II} phase, the texture of the Φ_R phase at 160 °C (Figure 11b) is significantly smaller than that obtained during cooling (Figure 10b). This is common, as the liquid crystalline texture develops better upon cooling than upon heating.

Free-Energy Diagram for the Phase Transitions. As has been discussed, there are five phases involved in HOBT-C8: the isotropic melt and the N_D, Φ_R, K_I, and K_{II} phases. Diagrams plotted between the Gibbs free energy (G) and the temperature to illustrate phase relationships are shown in parts a and b of Figure 12 upon cooling and heating, respectively. The corresponding DSC curves scanned at 10 °C/min are also included in this figure.

Thermodynamically, a system prefers a stable phase with the lowest free energy at a specific temperature and pressure. However, kinetically, the system may first go to a metastable phase with a local free energy minimum, depending upon the height of the free energy barriers of the phase transitions.[40,41] The discotic LC

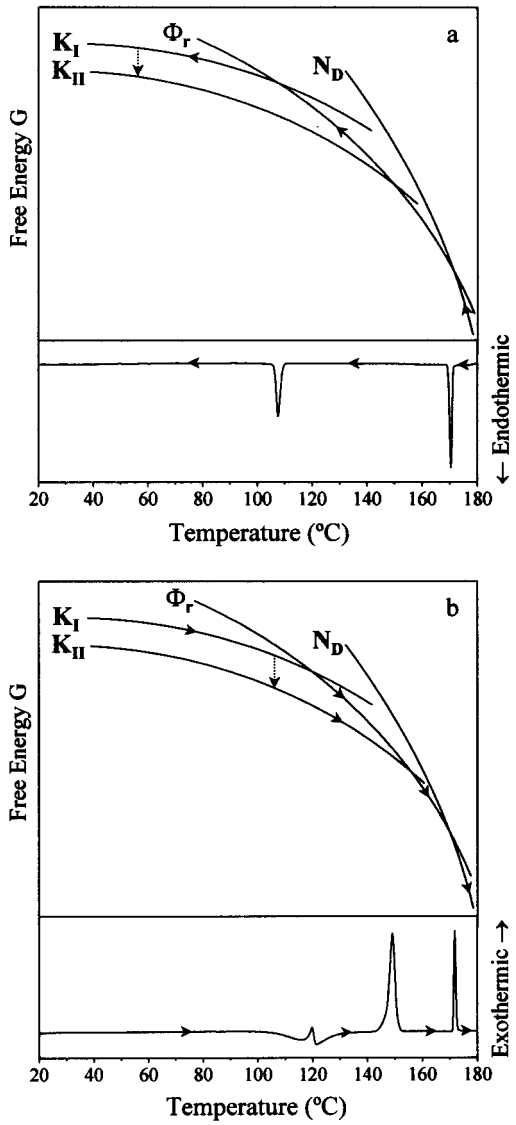

Figure 12. Phase diagrams of the free energy G versus the temperature for the phases and transitions of HOBT-C8: (a) during cooling; and (b) during subsequent heating. The corresponding DSC curves during cooling (a) and heating (b) at 10 °C/min are also included.

HOBT-C8 studied here provides an additional example. During fast cooling, the discotic HOBT-C8 exhibits the N_D phase and the Φ_R phase and bypasses the more stable K_{II} phase and enters directly the K_I phase (Figure 12a) due to a nucleation process in forming the K_{II} phase. Instead, HOBT-C8 goes into the K_I phase, which requires a lower free energy barrier. Only when the cooling rate is as slow as 1 °C/min can the K_{II} phase start to develop from the K_I phase, as evidenced in Figure 1.

During heating at a rate slower than 80 °C/min (Figure 2), the metastable K_I phase transfers to the K_{II} phase, partially or totally, depending on the heating rate. It seems that this transformation process can be carried out either by melting−recrystallization at a relatively fast heating rate or by a reorganization process at a relatively slow heating rate (Figure 2). Further heating leads to melting the K_{II} phase and transition to the Φ_R phase and, finally, the N_D phase (Figure 12b). Therefore, parts a and b of Figure 12 indicate that the K_I phase is monotropic with respect

(40) Cheng, S. Z. D.; Keller, A. *Annu. Rev. Mater. Sci.* **1998**, *28*, 533.
(41) Keller, A.; Cheng, S. Z. D. *Polymer* **1998**, *39*, 4461.

to the K_{II} phase. The monotropic and thermodynamically metastable K_I phase is experimentally observable only when the stable K_{II} phase is bypassed by a relatively fast cooling.

Conclusion

In summary, discotic HOBT-C8 shows that this material possesses multiple phases and transitions. Four different ordered phases exist. They are the thermodynamically stable N_D, Φ_R, and K_{II} phases and a metastable K_I phase. The structural determinations have shown that the Φ_R phase possesses rectangular column packing and that the metastable K_I crystalline phase has an orthorhombic crystalline lattice with the dimensions $a = 5.14$ nm, $b = 4.66$ nm, $c = 4.55$ nm, and $\alpha = \beta = \gamma = 90°$. The crystalline K_{II} phase possesses a monoclinic unit cell with the dimensions $a = 5.39$ nm, $b = 4.29$ nm, $c = 1.94$ nm, $\alpha = \beta = 90°$, and $\gamma = 94.5°$. When the cooling rates are relatively fast, the K_{II} phase can be bypassed and the discotic HOBT-C8 crystallizes into the metastable K_I phase directly. However, the K_{II} phase develops during very slow cooling or subsequent heating and forms the most stable phase. Both melting−recrystallization and reorganization mechanisms are involved in the formation of the K_{II} phase during heating. Hence, the less stable K_I phase is monotropic in nature with respect to the more stable K_{II} phase, and its appearance is solely dependent upon kinetic reasons.

Acknowledgment. This work was supported by the NSF ALCOM Science and Technology Center (DMR-8920147) at Kent State University, Case Western Reserve University and University of Akron, NSF (DMR-9617030), and the Nitto Denko Corporation.

CM0006897